ANALYTICAL MODELS FOR PREDICTING THE WALL-PRESSURE SPECTRUM IN TURBULENT BOUNDARY LAYERS

A. Rokade[1,3], R. Sabatini[1], C. Bailly[1], N. Trafny[2], R. Chin[3]

[1] *Ecole Centrale de Lyon, CNRS, Université Lyon 1, INSA Lyon, LMFA UMR5509, 69130 Ecully, France*
[2] *Naval Group, Naval Research, Ollioules, France*
[3] *Adelaide University, School of Electrical and Mechanical Engineering, South Australia 5000, Australia*

Abstract

The study reported in this paper reviews three formulations for predicting the wall-pressure spectrum beneath a turbulent boundary layer and establishes their connection under a common set of assumptions. The model inputs required by the formulations are also examined, and predictions are presented for a zero-pressure-gradient turbulent boundary layer at a specific Reynolds number. Finally, the contributions of different wall-normal regions of the boundary layer to the wall-pressure spectrum are analyzed as a function of frequency.

Keywords: *Wall-pressure fluctuations, Turbulent Boundary layer, Wave number frequency spectrum, Analytical model*

1. Introduction

Wall-pressure fluctuations induced by turbulent flows constitute a major source of flow-induced structural vibrations and the associated radiated noise in a broad range of engineering applications. These include naval structures [1], [2], aircraft cabin noise, trailing-edge noise from aerodynamic lifting surfaces [3], fans, and wind turbines, among many others.

The work reported in this paper seeks to develop and assess computationally efficient predictive models for the wall-pressure spectrum that retain a strong physical basis, in contrast to purely empirical formulations. In line with this objective, three approaches are considered, namely those described by Grasso *et al.* [4], Peltier and Hambric [5], and Lysak [6] (see also earlier references therein), hereafter referred to as Formulations 1-3.

Corresponding author: *ajit.rokade@ec-lyon.fr.*

In the present paper, the three approaches are reviewed, and the connections between them are established. In particular, it is shown that the three final expressions for the wall-pressure spectrum can be recovered from one another through appropriate assumptions (Sec. 2). The mean-flow and turbulence quantities required as inputs to the formulations are subsequently discussed (Sec. 3). The formulations are then applied to a zero-pressure-gradient turbulent boundary layer at a specific Reynolds number, and their predictions are compared with experimental data (Sec. 4). Finally, their integral structure is exploited to investigate the contributions of different wall-normal regions of the boundary layer to the wall-pressure spectrum, providing insight into the regions responsible for wall-pressure fluctuations across different frequency ranges.

2. Review of three formulations

A Cartesian coordinate system (x_1, x_2, x_3) is adopted, where x_1, x_2, and x_3 denote the streamwise, wall-normal, and spanwise directions, respectively.

The wall-pressure spectrum, $S_{pp}(\omega)$, is defined as the temporal Fourier transform of the wall-pressure auto-correlation function,

$$S_{pp}(\omega) = \frac{1}{2\pi}\int_{-\infty}^{+\infty} \overline{p'(\boldsymbol{x}_w, t)\, p'(\boldsymbol{x}_w, t+\tau)}\, e^{i\omega\tau}\,\mathrm{d}\tau, \quad (1)$$

where ω is the angular frequency, p' the pressure fluctuation, $\boldsymbol{x}_w$ an arbitrary point on the wall, t a reference time, and the overline denotes temporal averaging. By Parseval's theorem,

$$\overline{p'^2} = \int_{-\infty}^{+\infty} S_{pp}(\omega)\,\mathrm{d}\omega. \quad (2)$$

The starting point of all three formulations is the

Poisson equation governing incompressible pressure fluctuations [7], [8],

$$\nabla^2 p' = -(\Lambda_r + \Lambda_s), \tag{3}$$

where Λ_r and Λ_s denote the rapid and slow source terms, respectively. The rapid source results from the interaction between turbulent fluctuations and the mean velocity gradients, whereas the slow source is associated with turbulence-turbulence interactions. Following most previous studies [9], only the rapid source term is retained,

$$\Lambda_r = 2\rho \frac{\mathrm{d}\bar{U}_1}{\mathrm{d}x_2}\frac{\partial u_2'}{\partial x_1}, \tag{4}$$

where $\bar{U}_1(x_2)$ denotes the mean streamwise velocity, u_2' the wall-normal velocity fluctuation, and ρ the fluid density. The pressure field satisfies the Neumann boundary condition

$$\frac{\partial p'}{\partial x_2} = 0, \qquad x_2 = 0.$$

The three formulations reviewed in this paper differ only in the mathematical treatment of Eq. (3). In all cases, the turbulent velocity field is assumed to be statistically stationary and homogeneous in the wall-parallel directions, and Taylor's frozen-turbulence hypothesis is adopted.

2.1. Formulation 1

Formulation 1 follows the approach described by Grasso *et al.* [4]. Equation (3) is first Fourier transformed along the homogeneous axes (x_1, x_3), yielding a one-dimensional Helmholtz equation in the wall-normal direction. This equation is solved using the one-dimensional Green's function satisfying the Neumann boundary condition at the wall, leading to an integral representation of the transformed pressure fluctuation $p'(\boldsymbol{k}_\perp, x_2, t)$, where $\boldsymbol{k}_\perp = (k_1, k_3)$ denotes the wall-parallel wavenumber vector. The wall-pressure wavenumber spectrum, $\Phi_{pp}(\boldsymbol{k}_\perp, \tau)$, is then obtained from the pressure autocorrelation in the transformed domain. Finally, integrating over the wall-parallel wavenumbers and applying a temporal Fourier transform yields

$$\begin{aligned} S_{pp}^{(1)}(\omega) = 4\rho^2 \int_{-\infty}^{+\infty}\int_{0}^{\infty}\int_{-x_2}^{\infty} \frac{\omega^2 e^{-k_\perp[2x_2+\xi_2]}}{U_c^3(x_2+\xi_2)\,k_\perp^2} \left.\frac{\mathrm{d}\bar{U}_1(\eta)}{\mathrm{d}\eta}\right|_{\eta=x_2} \\ \times \left.\frac{\mathrm{d}\bar{U}_1(\eta)}{\mathrm{d}\eta}\right|_{\eta=x_2+\xi_2} \phi_{22}\big(\boldsymbol{k}_\perp, x_2, \xi_2\big)\,\mathrm{d}\xi_2\,\mathrm{d}x_2\,\mathrm{d}k_3, \end{aligned} \tag{5}$$

where

$$k_\perp = \sqrt{k_1^2 + k_3^2}, \qquad k_1 = \frac{\omega}{U_c(x_2+\xi_2)}, \tag{6}$$

and U_c denotes the convection velocity. The quantity ϕ_{22} is the two-dimensional cross-spectrum of the wall-normal velocity fluctuations,

$$\begin{aligned} \phi_{22}(\boldsymbol{k}_\perp, x_2, \xi_2) = \frac{1}{4\pi^2}\iint_{-\infty}^{+\infty} \overline{u_2'(\boldsymbol{x},t)u_2'(\boldsymbol{x}+\boldsymbol{\xi},t)} \\ \times e^{-i\boldsymbol{k}_\perp\cdot\boldsymbol{\xi}_\perp}\,\mathrm{d}\boldsymbol{\xi}_\perp, \end{aligned} \tag{7}$$

where $\boldsymbol{\xi} = (\xi_1, \xi_2, \xi_3)$ is the separation vector and $\boldsymbol{\xi}_\perp = (\xi_1, \xi_3)$ its wall-parallel component. The dependence of ϕ_{22} on both the reference position x_2 and the wall-normal separation ξ_2 reflects the inhomogeneity of the turbulent velocity field in the wall-normal direction.

2.2. Formulation 2

Formulation 2 follows the approach described by Peltier and Hambric [5]. The derivation starts from an integral representation of the fluctuating pressure field, $p'(\boldsymbol{x}, t)$, obtained from the three-dimensional Green's function satisfying the Neumann boundary condition at the wall. The wall-pressure autocorrelation function (see Eq. (1)) is then constructed, leading to a septuple integral over the source position $\boldsymbol{x}$, the separation vector $\boldsymbol{\xi}$, and the time lag τ.

To simplify the resulting expression, it is assumed that, for a given reference position x_2, the cross-spectrum $\phi_{22}(\boldsymbol{k}_\perp, x_2, \xi_2)$ decays rapidly with the wall-normal separation ξ_2. Consequently, the dominant contribution to the integral arises from the vicinity of $\xi_2 = 0$, allowing the approximations

$$\begin{aligned} U_c(x_2+\xi_2) &\simeq U_c(x_2), \\ \left.\frac{\mathrm{d}\bar{U}_1}{\mathrm{d}\eta}\right|_{x_2} \left.\frac{\mathrm{d}\bar{U}_1}{\mathrm{d}\eta}\right|_{x_2+\xi_2} &\simeq \left.\frac{\mathrm{d}\bar{U}_1}{\mathrm{d}\eta}\right|_{x_2}^2. \end{aligned} \tag{8}$$

A second approximation consists in neglecting the effect of the near-wall region to the wall-pressure spectrum. Consequently, only reference positions x_2 sufficiently far from the wall contribute significantly to the integral. For such positions, $\phi_{22}(\boldsymbol{k}_\perp, x_2, \xi_2)$ is negligible in the vicinity of the wall ($\xi_2 = -x_2$) and may therefore be regarded as a function of ξ_2 defined over the entire real line by extending it with zero values outside its effective support. The Fourier inversion theorem may then be applied, yielding

$$\phi_{22}(\boldsymbol{k}_\perp, x_2, \xi_2) = \int_{-\infty}^{+\infty} \phi_{22}(\boldsymbol{k}_\perp, x_2, k_2) e^{ik_2\xi_2}\,\mathrm{d}k_2, \tag{9}$$

where $\phi_{22}(\boldsymbol{k}_\perp, x_2, k_2)$ denotes the wall-normal component of the three-dimensional spectral tensor of velocity fluctuations. Although defined in the wavenumber space, this spectrum remains local since it is parameterized by the reference position x_2.

These approximations considerably simplify the resulting expression, yielding

$$S_{pp}^{(2)}(\omega) = 4\rho^2 \int_0^{+\infty} \frac{\omega^2}{\bar{U}_1^3(x_2)} \left.\frac{\mathrm{d}\bar{U}_1(\eta)}{\mathrm{d}\eta}\right|^2_{\eta=x_2} \times \left[\iint_{-\infty}^{+\infty} \frac{e^{-[k_\perp + \mathrm{i}k_2]x_2}}{k_\perp^2 \, [k_\perp - \mathrm{i}k_2]} \phi_{22}(\boldsymbol{k}_\perp, x_2, k_2) \, \mathrm{d}k_2 \, \mathrm{d}k_3 \right] \mathrm{d}x_2. \tag{10}$$

where $k_\perp = (k_1^2 + k_3^2)^{1/2}$, with k_1 given by Eq. (6).

2.3. Formulation 3

Formulation 3 follows the approach proposed by Lysak [6]. The derivation begins with an integral representation of the fluctuating pressure field, $p'(\boldsymbol{x}, t)$, obtained using the three-dimensional Green's function satisfying the Neumann boundary condition at the wall. A Fourier transform is then applied in the homogeneous directions (x_1, x_3) and in time, yielding the transformed wall-pressure fluctuation $p'(\boldsymbol{k}_\perp, x_2 = 0, \omega)$. The wall-pressure wavenumber-frequency spectrum, $\Phi_{pp}(\boldsymbol{k}_\perp, \omega)$, is subsequently derived through a lengthy sequence of non-obvious analytical manipulations, which are beyond the scope of the present paper, and expressed in terms of the cross-spectrum ϕ_{22} evaluated at $k_2 = 0$, namely $\phi_{22}(\boldsymbol{k}_\perp, x_2, k_2 = 0)$.

As in Formulation 2, obtaining this expression requires assuming that the cross-spectrum $\phi_{22}(\boldsymbol{k}_\perp, x_2, \xi_2)$ decays rapidly with the wall-normal separation ξ_2, thereby allowing the same simplifying approximations. In addition, $\phi_{22}(\boldsymbol{k}_\perp, x_2, \xi_2)$ is supposed to be an even function of ξ_2, which further simplifies the resulting expression. The wall-pressure spectrum is finally given by

$$S_{pp}^{(3)}(\omega) = 8\pi\rho^2 \int_0^{\infty} \left(\frac{\mathrm{d}\bar{U}_1}{\mathrm{d}x_2}\right)^2 \frac{\omega^2}{U_c^3(x_2)} \times \left[\int_{-\infty}^{+\infty} \frac{e^{-2k_\perp x_2}}{k_\perp^2} \phi_{22}(\boldsymbol{k}_\perp, x_2, k_2 = 0) \, \mathrm{d}k_3 \right] \mathrm{d}x_2. \tag{11}$$

where $k_\perp = (k_1^2 + k_3^2)^{1/2}$, with k_1 given by Eq. (6).

2.4. Connection between the formulations

Although derived using different mathematical approaches, the three formulations are closely related. Formulation 1 is the most general, relying only on the assumptions that the turbulent velocity field is statistically stationary, homogeneous in the wall-parallel directions, and satisfies Taylor's frozen-turbulence hypothesis. Formulations 2 and 3 are recovered from Formulation 1 through the successive introduction of additional simplifying assumptions, as demonstrated below.

2.4.1. From Formulation 1 to Formulation 2

Upon substituting the approximations (8) and the Fourier representation (9) into Eq. (5), the following expression is obtained:

$$S_{pp}^{(1)}(\omega) \simeq 4\rho^2 \int_0^{\infty} \frac{\omega^2}{U_c^3(x_2)} \left.\frac{\mathrm{d}\bar{U}_1(\eta)}{\mathrm{d}\eta}\right|^2_{\eta=x_2} \times \left[\iint_{-\infty}^{+\infty} \frac{\phi_{22}(\boldsymbol{k}_\perp, x_2, k_2)}{k_\perp^2} \times \left(\int_{-x_2}^{\infty} e^{-k_\perp[2x_2+\xi_2] + ik_2\xi_2} \, \mathrm{d}\xi_2 \right) \mathrm{d}k_2 \, \mathrm{d}k_3 \right] \mathrm{d}x_2. \tag{12}$$

The inner integral can be evaluated analytically, yielding Eq. (10). Formulation 2 is therefore recovered from Formulation 1, *i.e.*, $S_{pp}^{(1)} \simeq S_{pp}^{(2)}$.

2.4.2. From Formulation 1 to Formulation 3

Introducing the approximations (8) into Eq. (5) gives the following expression:

$$S_{pp}^{(1)}(\omega) \simeq 4\rho^2 \int_{-\infty}^{+\infty} \int_0^{\infty} \frac{\omega^2 e^{-2k_\perp x_2}}{U_c^3(x_2)\, k_\perp^2} \left.\frac{\mathrm{d}\bar{U}_1(\eta)}{\mathrm{d}\eta}\right|^2_{\eta=x_2} \times \left(\int_{-x_2}^{\infty} \phi_{22}\big(\boldsymbol{k}_\perp, x_2, \xi_2\big) e^{-k_\perp \xi_2} \, \mathrm{d}\xi_2 \right) \mathrm{d}x_2 \, \mathrm{d}k_3. \tag{13}$$

Since ϕ_{22} is assumed to decay rapidly with the wall-normal separation ξ_2, the dominant contribution to the inner integral arises from the neighbourhood of $\xi_2 = 0$. In this neighbourhood, the exponential factor may therefore be approximated by its first-order Taylor expansion about $\xi_2 = 0$,

$$e^{-k_\perp \xi_2} \simeq 1 - k_\perp \xi_2.$$

In Formulation 3, $\phi_{22}(\boldsymbol{k}_\perp, x_2, \xi_2)$ is further assumed to be an even function of ξ_2. Together with the rapid decay of ϕ_{22}, this symmetry implies that, for reference positions sufficiently far from the wall, the contribution associated with the linear term in the Taylor expansion vanishes. By neglecting the contribution of the near-wall region, the lower integration limit can again be extended from $-x_2$ to $-\infty$. Using the identity

$$\int_{-\infty}^{+\infty} \phi_{22}\big(\boldsymbol{k}_\perp, x_2, \xi_2\big) \, \mathrm{d}\xi_2 = 2\pi \, \phi_{22}(\boldsymbol{k}_\perp, x_2, k_2 = 0), \tag{14}$$

Eq. (11) is finally recovered, *i.e.*, $S_{pp}^{(1)} \simeq S_{pp}^{(3)}$.

3. Mean flow and turbulence inputs

All the formulations introduced in Sec. 2 require the streamwise mean velocity profile $\bar{U}_1(x_2)$, an expression for the convection velocity U_c, and a model for the spectral tensor component ϕ_{22}. The mean velocity profile $\bar{U}_1(x_2)$ is computed using a one-dimensional approach based on a mixing-length model, by integrating an ordinary differential equation along the wall-normal direction x_2 [10]. The governing equations are not repeated here; however, the model has been extended to account for the effects of a mean pressure gradient. Further details are provided in a companion paper [11].

The convection velocity U_c is assumed to be equal to the mean streamwise velocity.

A local analytical description of turbulence is required to evaluate the spectral tensor component ϕ_{22}. In this work, the von Kármán model [12] is adopted for the turbulent kinetic energy $E(k)$,

$$E(k) = \alpha \, u'^2 L_e \, \frac{(kL_e)^4}{[1 + (kL_e)^2]^{17/6}}, \tag{15}$$

where u'^2 denotes the variance of the velocity fluctuations and L_e is the integral length scale. The constant α is determined by requiring that integration of $E(k)$ over $k \in \mathbb{R}^+$ recovers the turbulent kinetic energy $(3/2)u'^2$, yielding

$$\alpha = \frac{55}{9\sqrt{\pi}} \frac{\Gamma\left(\frac{5}{6}\right)}{\Gamma\left(\frac{1}{3}\right)}.$$

The length scale L_e is linked by definition to the longitudinal integral length scale L_1 by

$$L_1 = \sqrt{\pi}\, \Gamma(5/6)/\Gamma(1/3) \, L_e \tag{16}$$

At each wall-normal position x_2 within the boundary layer, the turbulence is assumed to be locally homogeneous and isotropic. From Eq. (15), the spectral tensor component ϕ_{22} is expressed in Fourier space as

$$\phi_{22}(\boldsymbol{k}) = \frac{\alpha u'^2 L_e^3}{4\pi} \, \frac{(k_\perp L_e)^2}{[1 + (kL_e)^2]^{17/6}}. \tag{17}$$

It is worth recalling that the spectral tensor is defined as the Fourier transform of the correlation function $R_{22}(\boldsymbol{\xi})$ [13]. Turbulence is only formally homogeneous in plane $(x_1 - x_3)$. The two-dimensional cross-spectrum $\phi_{22}(\boldsymbol{k}_\perp, x_2, \xi_2)$ is thus introduced where x_2 is the running point along the normal direction to the wall and ξ_2 the separation, as already introduced in Section 2. For the von Kármán model (15), one has

$$\begin{aligned} \phi_{22}(\boldsymbol{k}_\perp, x_2, \xi_2) \quad &= \quad \frac{u'^2 L_e^4 k_\perp^2}{\Gamma(1/3)\, \pi \, 2^{4/3}} \\ &\times \quad \frac{\xi^{7/3} \, K_{7/3}(\xi)}{[1 + (k_\perp L_e)^2]^{7/3}}, \end{aligned} \tag{18}$$

where $\xi = (|\xi_2|/L_e)[1 + (k_\perp L_e)^2]^{1/2}$ is an auxiliary variable, Γ is the gamma function and K denotes the modified Bessel function of the second kind. Expression (17) is retrieved by taking the Fourier transform of (18) for homogeneous turbulence along the x_2 direction [14].

In Eq. (18), the quantities u'^2 and L_e are local quantities that vary with x_2. Their variation is, however, assumed to be negligible over the correlation length associated with the separation ξ_2 at a given x_2 location, so that the assumptions of local homogeneity and isotropy underlying the turbulence model remain valid.

The variance of velocity fluctuations is taken to be equal to the wall-normal velocity variance, $u'^2 = \overline{u_2'^2}(x_2)$. Based on experimental data in the logarithmic region [15], the relation $\overline{u_2'^2} \simeq 1.3\, \overline{u_1' u_2'}$ is assumed. Introducing the mixing length $l_m(x_2)$ yields [10]

$$\overline{u_2'^2} \simeq 1.3 \, (l_m \, d\bar{U}_1/dx_2)^2. \tag{19}$$

The velocity fluctuations along the x_2 direction are thus obtained as a byproduct of the determination of the mean velocity profile $\bar{U}_1$. Note that there is a misprint in Prigent and Bailly [10], where the square is missing in their Eq. (13). The mixing length l_m is directly provided by the model used to compute the mean velocity profile and is also used to determine the evolution of L_e, and thus of L_1, through Eq. (16). Following [10], $L_e(x_2)$ is calculated as

$$L_e(x_2) = \frac{l_m(x_2)}{(\sqrt{\pi}/2)\Gamma(5/6)/\Gamma(1/3)} \simeq \frac{l_m(x_2)}{0.37}, \tag{20}$$

in fair agreement with the estimate $l_m \simeq 0.31 L_1$ proposed, for instance, by Lysak [6].

In the present model, the mixing length l_m and the mean streamwise velocity profile $\bar{U}_1$ are fully determined by the Reynolds number $\mathrm{Re}^+ = u_\tau \delta/\nu$, where u_τ is the friction velocity, δ is the boundary layer thickness, and ν is the fluid's kinematic viscosity. Consequently, the convection velocity U_c, the wall-normal velocity variance $\overline{u_2'^2}$, the integral length scale L_e, and ultimately the spectral tensor component ϕ_{22} also depend only on Re^+. Thus, Re^+ is the only parameter required to characterize the input quantities entering the wall-pressure spectrum formulations. It represents the ratio of the boundary-layer thickness δ to the viscous length scale $l_\nu = \nu/u_\tau$. Quantities normalized using u_τ and l_ν as velocity and length scales, respectively, are conventionally denoted by the superscript +; in particular, $\delta^+ = \mathrm{Re}^+$, also known as the Kármán number.

4. Results

The mean velocity profile $\bar{U}_1$, the rms value of the transverse velocity fluctuations u_2' and the length scale L_e are plotted in Fig. 1 for $\mathrm{Re}_+ = 2369$, corresponding to the highest Reynolds number zero-pressure gradient turbulent boundary layer considered in the experimental study of Gravante *et al.* [16]. The mean velocity is in agreement with other experimental investigations, while the variance is a direct consequence of Eq. (19). The evolution of L_e^+ is related to the mixing length l_m^+ used to compute the mean velocity profile. As expected, the turbulent fluctuations vanish at the edge of the boundary layer, that is at $x_2^+ = \delta^+ = \mathrm{Re}^+$.

The predicted normalized wall-pressure spectra, $S_{pp}^+(\omega^+) = S_{pp}(\omega)/(\nu\rho^2 u_\tau^2)$, with $\omega^+ = \omega\nu/u_\tau^2$, are

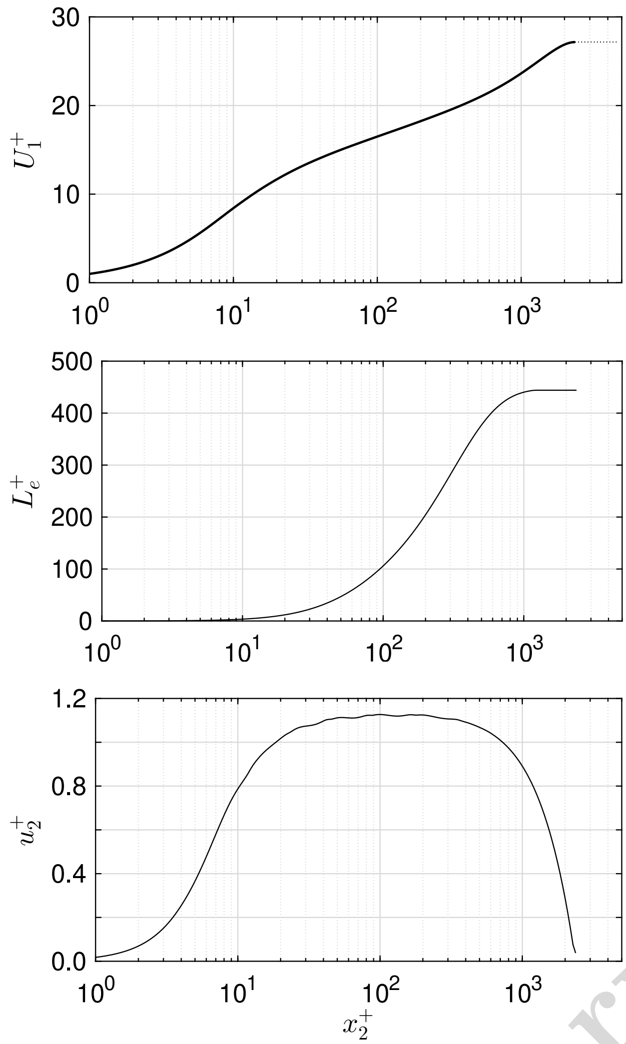

Figure 1: Transverse profiles of the input quantities used in analytical models for $\mathrm{Re}_+ = 2369$: (a) mean velocity $\bar{U}_1^+$, (b) length scale L_e^+ and (c) rms of the transverse fluctuating velocity $u_2'^+$.

compared with the measurements of Gravante *et al.* [16] in Fig. 2. The spectra obtained with Formulations 2 and 3 are represented by the red dashed and blue solid lines, respectively. The two predictions exhibit a similar overall shape, with the spectral peak occurring at approximately the same frequency, $\omega^+ \simeq 0.03$. Differences are observed, however, in the amplitude near the peak and in the high-frequency decay. These differences are also reflected in the root-mean-square value of the wall fluctuating pressure. The measurements yield $p'^+ \simeq 2.9$, compared with $p'^+ \simeq 2.1$ and $p'^+ \simeq 2.5$ for Formulations 2 and 3, respectively.

The formulations 1-3 involve an integration across the boundary layer, making it possible to identify the contribution of each wall-normal region to the wall-pressure spectrum as a function of frequency. As an illustration, a map obtained using Formulation 3 is shown in Fig. 3 as a function of (ω^+, x_2^+). The horizontal dashed lines delineate the different regions of the turbulent boundary layer, as indicated on the left of the panel. At each frequency, the black symbols $\times$ indicate the wall-normal location at which the contribution to the wall-pressure spectrum reaches its maximum. A clear frequency dependence of this location is observed. As the frequency increases, the maximum contribution progressively shifts toward the wall, whereas the low-frequency contributions originate predominantly from the outer regions of the boundary layer. The source intensity is closely correlated with the $\overline{u_2'^2}$ profile, and the dominant contribution originates from the logarithmic region, which expands with increasing Reynolds number.

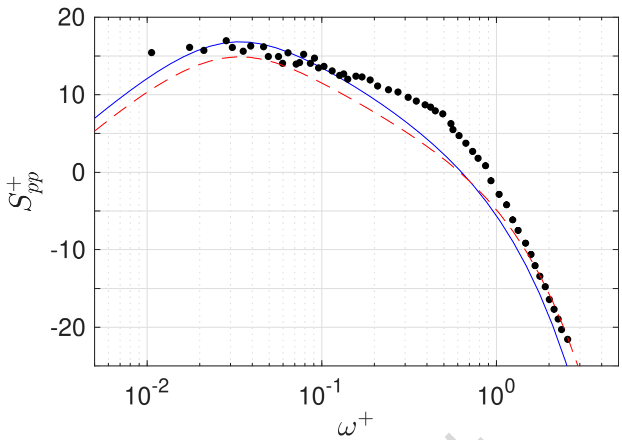

Figure 2: Predicted wall-pressure spectrum for $\mathrm{Re}_+ = 2369$: • measurements [16]; - - - Formulation 2 (10); —— Formulation 3 (11).

5. Conclusion

In this study, three formulations for predicting the wall-pressure spectrum in turbulent boundary layers have been reviewed, and the relationships between them have been established under a common set of assumptions. This work is currently being extended by incorporating the effects of a mean pressure gradient and the contribution of the nonlinear (slow) source term. It has also been shown that a more detailed characterization of the contribution of each wall-normal layer to the wall-pressure spectrum is possible, providing a basis for refining the model to account for the missing contributions from the near-wall and wake regions.

6. Acknowledgement

The present work is Co-funded by the European Union under the Marie Skłodowska-Curie Grant Agreement No 101081465 (AUFRANDE). Views and opinions expressed are however those of the authors only and do not necessarily reflect those of the European Union or the Research Executive Agency. Neither the European Union nor the Research Executive Agency can be held responsible for them.

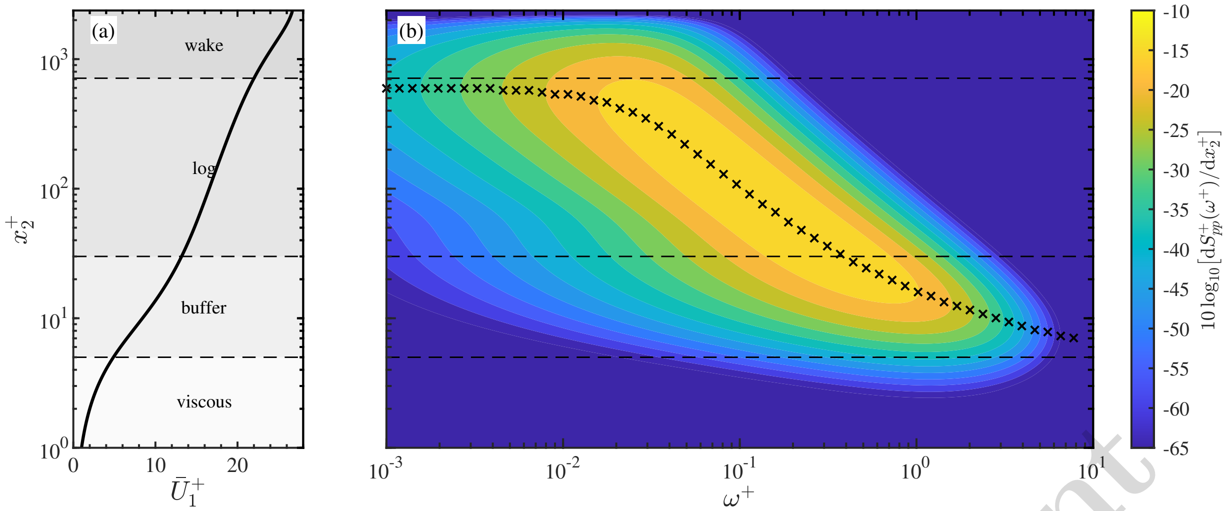

Figure 3: Contribution of each boundary-layer region to the wall-pressure footprint, for $\mathrm{Re}_+ = 2369$; (a) mean velocity profile, (b) map of dS^+_{pp}/dx^+_2 in the (ω^+, x^+_2) plane, where the black crosses indicate the wall-normal locations of the maximum contribution at each frequency.

References

[1] N. Trafny, G. Serre, B. Cotté, and J.-F. Mercier, "A stochastic volume approach based on tailored Green's functions for airfoil noise prediction at low mach number," *Journal of Sound and Vibration*, vol. 551, p. 117 603, 2023.

[2] Y.-T. Lee, W. K. Blake, and T. M. Farabee, "Modeling of wall pressure fluctuations based on time mean flow field," *Journal of Fluids Engineering*, vol. 127, no. 2, pp. 233–240, Sep. 2004.

[3] S. Lee, L. Ayton, F. Bertagnolio, S. Moreau, T. P. Chong, and P. Joseph, "Turbulent boundary layer trailing-edge noise: Theory, computation, experiment, and application," *Progress in Aerospace Sciences*, vol. 126, p. 100 737, 2021.

[4] G. Grasso, P. Jaiswal, H. Wu, S. Moreau, and M. Roger, "Analytical models of the wall-pressure spectrum under a turbulent boundary layer with adverse pressure gradient," *J. Fluid Mech.*, vol. 877, pp. 1007–1062, 2019.

[5] L. J. Peltier and S. A. Hambric, "Estimating turbulent-boundary-layer wall-pressure spectra from CFD RANS solutions," *J. Fluids Struct.*, vol. 23, no. 6, pp. 920–937, 2007.

[6] P. D. Lysak, "Modeling the wall pressure spectrum in turbulent pipe flows," *J. Fluids Eng.*, vol. 128, no. 2, pp. 216–222, 2006.

[7] R. H. Kraichnan, "Pressure fluctuations in turbulent flow over a flat plate," *J. Acoust. Soc. Am.*, vol. 28, no. 3, pp. 378–390, 1956.

[8] G. M. Lilley, "Pressure fluctuations in an incompressible turbulent boundary layer," The College of Aeronautics, Cranfield, U.K., Rep. 133, 1960.

[9] T. F. Rossi and P. Sagaut, "Prediction of wall-pressure spectra for separated/reattached boundary layer flows," in *AIAA AVIATION 2023 Forum*, 2023.

[10] S. L. Prigent and C. Bailly, "From shear stress to wall pressure spectra: A semi-analytical approach to account for mean pressure gradients in turbulent boundary layers," *Acta Acustica*, vol. 6, p. 43, 2022. DOI: 10.1051/aacus/2022034

[11] A. Rokade, R. Sabatini, C. Bailly, N. Trafny, and R. Chin, "Robustness of analytical models for predicting wall pressure spectrum in turbulent boundary layers," *to appear in Ercoftac Bulletin*, 2026.

[12] T. v. Kármán, "Progress in the statistical theory of turbulence," *Proc. Natl. Acad. Sci. U.S.A.*, vol. 34, pp. 530–539, 1948.

[13] C. Bailly and G. Comte-Bellot, *Turbulence*. Springer International Publishing Switzerland, 2015.

[14] D. K. Wilson, "Three-dimensional correlation and spectral functions for turbulent velocities in homogeneous and surface-blocked boundary layer," Army Research Laboratory, ARL-TR-1287, 1997.

[15] B. Aupoix, "Extension of Lysak's approach to evaluate the wall pressure spectrum for boundary layer flows," *Flow Turbul. Combust.*, vol. 94, pp. 63–78, 2015. DOI: 10.1007/s10494-014-9538-4

[16] S. P. Gravante, A. M. Naguib, C. E. Wark, and H. M. Nagib, "Characterization of the pressure fluctuations under a fully developed turbulent boundary layer," *AIAA J.*, vol. 36, no. 10, pp. 1808–1816, 1998. DOI: 10.2514/2.296